Bachelor's Thesis

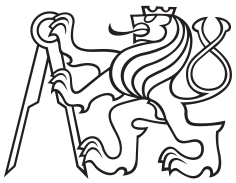

Czech Technical University in Prague

F3

Faculty of Electrical Engineering
Department of Measurement

Development of an Electrochemical Impedance Spectroscopy (EIS) Measurement System with Active Current Excitation for Online Battery Monitoring

Tom Pastuszek

Supervisor: Ing. Tomáš Haubert, Ph.D.
Field of study: Cybernetics and Robotics
January 2024

ZADÁNÍ BAKALÁŘSKÉ PRÁCE

I. OSOBNÍ A STUDIJNÍ ÚDAJE

Příjmení: **Pastuszek** Jméno: **Tom** Osobní číslo: **483990**

Fakulta/ústav: **Fakulta elektrotechnická**

Zadávající katedra/ústav: **Katedra měření**

Studijní program: **Kybernetika a robotika**

II. ÚDAJE K BAKALÁŘSKÉ PRÁCI

Název bakalářské práce:

Vývoj měřícího systému elektrochemické impedanční spektroskopie (EIS) s aktivním proudovým buzením pro online monitorování baterií

Název bakalářské práce anglicky:

Development of an Electrochemical Impedance Spectroscopy (EIS) Measurement System with Active Current Excitation for Online Battery Monitoring

Pokyny pro vypracování:

1. Research battery management systems (BMSs) and EIS for EV batteries.
2. Design an active current excitation circuit for online battery EIS. Apply this circuit with laboratory test equipment to measure the impedance spectra of lithium-ion battery cells.
3. Develop a microcontroller-based EIS system prototype that manages the current excitation circuit, acquires current and voltage measurements, and generates the battery impedance spectra.

Seznam doporučené literatury:

[1] D. Faktorová, M. Kuba, S. Pavlíková, and P. Fabo, “Implementation of the impedance spectroscopy using a modern microcontroller,” Procedia Structural Integrity, vol. 43, pp. 288-293, 2023.
[2] Q. Yao, D.-D.-C. Lu, and G. Lei, “Accurate online battery impedance measurement method with low output voltage ripples on power converters,” Energies, vol. 14, no. 4, p. 1064, Feb. 2021.
[3] P. Haussmann, J. J. Melbert, "Sensorless individual cell temperature measurement by means of impedance spectroscopy using standard battery management systems of electric vehicles," SAE Technical Paper 2020-01-0863, 2020.
[4] A. Howey, P. D. Mitcheson, V. Yufit, G. J. Offer and N. P. Brandon, "Online measurement of battery impedance using motor controller excitation," IEEE Transactions on Vehicular Technology, vol. 63, no. 6, pp. 2557-2566, July 2014.
[5] A. Christensen and A. Adebusuyi, "Using on-board electrochemical impedance spectroscopy in battery management systems," 2013 World Electric Vehicle Symposium and Exhibition (EVS27), Barcelona, Spain, pp. 1-7, 2013.

Jméno a pracoviště vedoucí(ho) bakalářské práce:

Ing. Tomáš Haubert, Ph.D. katedra elektrických pohonů a trakce FEL

Jméno a pracoviště druhé(ho) vedoucí(ho) nebo konzultanta(ky) bakalářské práce:

Datum zadání bakalářské práce: **14.09.2023** Termín odevzdání bakalářské práce: **09.01.2024**

Platnost zadání bakalářské práce:
do konce zimního semestru 2024/2025

Ing. Tomáš Haubert, Ph.D. podpis vedoucí(ho) práce	podpis vedoucí(ho) ústavu/katedry	prof. Mgr. Petr Páta, Ph.D. podpis děkana(ky)

III. PŘEVZETÍ ZADÁNÍ

Student bere na vědomí, že je povinen vypracovat bakalářskou práci samostatně, bez cizí pomoci, s výjimkou poskytnutých konzultací.
Seznam použité literatury, jiných pramenů a jmen konzultantů je třeba uvést v bakalářské práci.

. _____
Datum převzetí zadání

_____
Podpis studenta

Acknowledgements

I would like to thank Ing. Tomáš Haubert, Ph.D., for his valuable suggestions and together with Porsche Engineering Services s.r.o. for the opportunity to work on this project. Additionally, I would like to express my gratitude to Ing. Aaron David Scher, MSc., Ph.D., for his intense consultations and positive approach. Lastly, I would like to thank my family and friends for their support during my studies.

Declaration

I declare that I have written, developed and implemented this thesis by myself and that I have listed all used sources according to the Guideline no. 1/2009 for adhering to ethical principles when elaborating an academic final thesis.

In Prague,

date	Tom Pastuszek

Abstract

This thesis elaborates on onboard battery electrochemical impedance spectroscopy (EIS) for lithium-ion battery cells used in electric vehicles. The main objective is the development and validation of a low voltage proof of concept. The research, conducted at Porsche Engineering Services s.r.o., involves creating a prototype using a voltage-controlled current sink to modulate the current that perturbs the battery cells and measuring the battery cell voltage to obtain the battery impedance data.

Two versions of the prototype are presented – one utilizing a laboratory device, the Bode 100 spectrum analyzer, and the other integrating an MCU, the STM32 F303RE Nucleo board. Both versions and their implementations are detailed in the thesis, emphasizing key aspects such as the main circuit board and EIS technique. Measurements were initially conducted with the Bode 100 at different state of charge and temperatures of the battery cell, comparing the resulting Nyquist plots of battery impedance with findings from other studies. Subsequently, measurement using the MCU revealed challenges associated with this implementation. Lastly, the thesis concludes with a discussion of the results, along with an exploration of the feasibility and challenges associated with the implementation.

Keywords: Electrochemical impedance spectroscopy, Battery management, Electric vehicles, circuit design, Microcontroller, Battery impedance, Nyquist plot, Lithium-ion battery

Supervisor: Ing. Tomáš Haubert, Ph.D.
Department of Electric Drives and Traction FEE

Abstrakt

Tato práce se zabývá palubní elektrochemickou impedanční spektroskopií lithium-iontových baterií používaných v elektromobilech. Hlavním cílem je vytvoření a ověření nízkonapěťového prototypu. Výzkum, realizovaný v Porsche Engineering Services s.r.o., zahrnuje vytvoření prototypu s použitím napěťově regulovaného proudového modulátoru, který budí bateriové články a měří jejich změnu napětí, na základě které se následně získá impedance baterie.

Dvě verze prototypu jsou vytvořeny – jedna používající laboratorní zařízení, spektrální analyzátor Bode 100, a druhá používající mikrokontroler STM32 F303RE Nucleo. Obě verze a jejich implementace jsou detailně popsány v práci, včetně návrhu obvodu a popisu použité techniky elektrochemické impedanční spektroskopie. Měření byla nejprve realizována s přístrojem Bode 100 při různých stavech nabití a teplotách bateriového článku, a získané Nyquistovy diagramy impedance jsou porovnány s daty z jiných studií. Následně bylo provedeno měření s použitím mikrokontroleru, které odhalilo problémy s jeho použitím a provedenou implementací. Nakonec práci uzavírá diskuse o výsledcích společně s průzkumem proveditelnosti a výzev spojenými s touto implementací.

Klíčová slova: Elektrochemická impedanční spektroskopie, Managment baterií, Elektrická vozidla, Návrh obvodu, Mikrokontroler, Impedance baterie, Nyqustův diagram, Lithium-iontová baterie

Překlad názvu: Vývoj měřícího systému elektrochemické impedanční spektroskopie (EIS) s aktivním proudovým buzením pro online monitorování baterií

Contents

Figures

Tables

Chapter 1

Introduction

Electrochemical impedance spectroscopy (EIS) is a commonly used technique for battery characterization through impedance measurements, offering useful information on battery performance and health. It is a non-destructive technique used to study and measure properties of various electrochemical systems and materials as a function of frequency. In the case of batteries, the impedance is usually presented as a Nyquist plot, with the real part on the x-axis and imaginary part on the y-axis. This data can be used to determine state of charge (SOC), state of health (SOH) and estimate the number of cycles of the battery. Typically, EIS measurements are performed in a controlled laboratory environment [1]. However, in recent years there is growing demand for accurate battery characterization and diagnostics for electric vehicles (EV). In this thesis the goal is to prototype an onboard EIS battery measurement system.

This thesis was performed at Porsche Engineering Services s.r.o. The goal of the prototype is to provide a low voltage proof of concept that can be scaled later to practical high voltage systems.

1.1 Introduction and motivation

The motivation of this thesis is to develop a simple and accurate prototype system for real-time (onboard) EIS measurements of lithium-ion batteries for electric vehicles. As the automotive industry is switching to electric vehicles (EVs), the focus is changing from combustion engines to electric motors and batteries. EV Battery management systems (BMS) are used to monitor and manage the performance and safety of the vehicle's battery, but traditionally rely on passive measurements of cell voltage and current. Onboard EIS offers a promising enhancement based on active impedance measurements. For example, EIS can be used to calculate SOC for charging the battery pack closer to its maximum capacity and increase the vehicle range [2].EIS data can also be used to calculate the remaining range of a vehicle more accurately. EIS can also support safety measures as it can provide better information about cell temperature to prevent overheating and possible ignition of the battery pack. These benefits have led to increasing interest and demand in

recent years for an onboard EIS and are the motivation for this work.

1.2 Main objective and partial tasks

The main objective of this thesis is to create an online EIS battery measurement system with active current excitation for online battery monitoring. Partial tasks of this thesis are:

- Research battery management systems (BMSs) and EIS for EV batteries.
- Design an active current excitation circuit for online battery EIS. Apply this circuit with laboratory test equipment to measure the impedance spectra of lithium-ion battery cells.
- Develop a microcontroller-based EIS system prototype that manages the current excitation circuit, acquires current and voltage measurements, and generates the battery impedance spectra.

Chapter 2

Background to EVs and battery management

2.1 EV introduction

The market for EVs has seen rapid growth in recent years, with a projected global revenue of up to 561.3 billion US dollars in 2023 [9]. By 2025, it is expected that 20% of all passenger vehicles sold worldwide will be electric. This percentage is anticipated to rise to 40% by 2030. Notably, the EU has proposed banning the sales of new vehicles with combustion engines to achieve a 100% market share for EVs in Europe by 2035, and other governments targeting the same goal by 2040 [10].

The main difference that distinguishes EVs from their combustion counterparts is the use of electric power to propel the vehicle instead of using combustion. Electric power is stored in the batteries and then used to power the traction motors. A DC-DC converter is used to convert voltage levels, facilitating the transfer of energy from and to the battery according to components' power requirements. To manage the battery, a battery management system (BMS) is used. It controls the charge and discharge of the cells in the battery pack, estimates the state-of-charge (SOH) and state-of-health (SOH), monitors the temperature and voltage of the battery cells, provides cell balancing, and disconnects the battery in case of an emergency. Another essential component of EVs is the thermal management system (TMS). This system not only cools the battery, powertrain, and other components, but can also heat the battery to operate at the maximum efficiency at startup (for example, in the winter months) and to support the charging process.

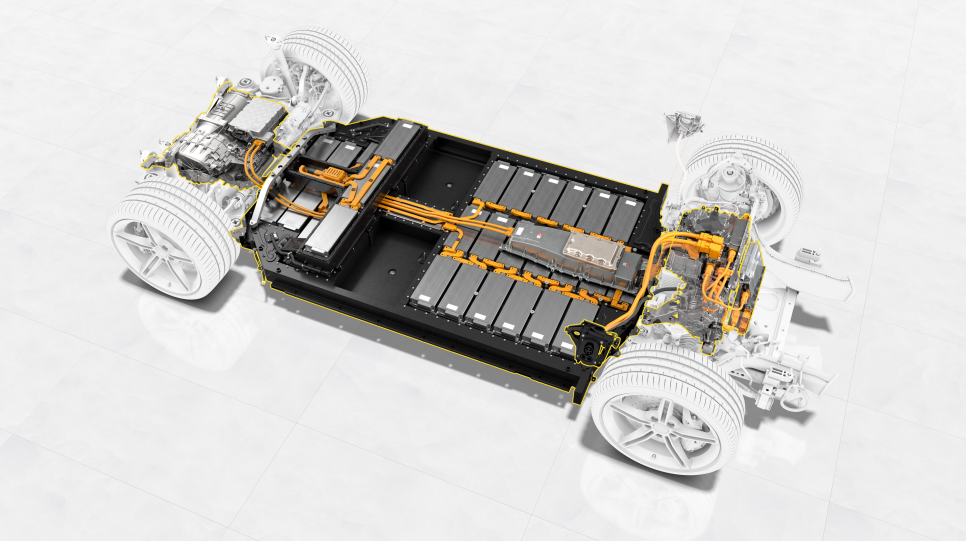

Figure 2.1: Porsche Taycan battery system - taken from[11]

2.2 EV battery management introduction

The battery of an EV usually consists of multiple battery packs that can be distributed throughout the car to provide needed space for occupants or to evenly distribute weight and balance the vehicle. Each battery pack contains individual battery cells and has its own BMS.

The battery management system is responsible for overseeing a battery pack. It measures the voltage of each cell in the pack, measures the current flowing to and from the pack and monitors the temperature with sensors distributed evenly throughout the pack. Based on this data, current EV BMSs passively estimate the SOC and SOH of the cells. One of the most common algorithms of estimation that is used within the BMS is Kalman filter. This algorithm provides estimation of parameters based on measurements observed over time [12].

Primarily, the BMS communicates with other components and exchanges information to manage the maximum current through the battery pack. Additionally, the BMS has the capability to predict potential errors to prevent failure of the battery pack and create hazard for the occupants of the vehicle. In case of an emergency, the BMS can disconnect the battery pack. The BMS also provides cell balancing to maintain uniform charge levels and extend the overall battery life.

Another crucial part in battery management is the thermal management system (TMS). TMS is responsible for maintaining the optimal thermal conditions for the battery and the entire system of the vehicle, ensuring maximum efficiency under varying external conditions. Not only does the TMS cool the

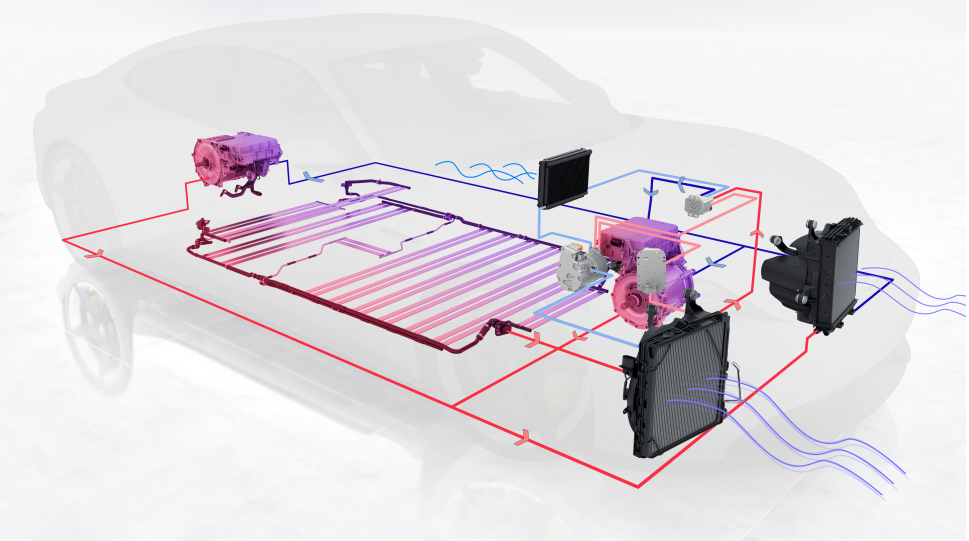

Figure 2.2: Porsche Taycan TMS - taken from[11]

components during driving and charging to prevent overheating, but it also preheats the battery before charging to ensure maximum charging current can be safely applied (in cold weather).

Currently, the most commonly used TMS technologies are air-based or indirect liquid-based. While these technologies may be sufficient, in recent years new technologies have emerged [13]. One of them is using direct oil, where the dielectric oil is used as the coolant, which offers the potential for efficient heat transfer with a more uniform and controlled temperature. However, due to the high viscosity of the oil, the cooling effect may not be significantly improving in all cases and this technology suffers from leaks caused by the liquid properties. Another improvement is to use nanoparticles of high thermally conductive metals such as copper or silver. According to a study [14], this can increase the thermal conductivity by 23.8%. An alternative solution uses liquid metals like gallium or mercury as coolant. However, this technology faces challenges due to weak pumping flow, as the traditional pumps struggle to circulate liquid metal through the system.

2.3 EIS for battery characterization

In general, to obtain battery characteristics, various destructive and non-destructive measuring methods exist. These techniques differ in terms of accuracy, measuring duration or complexity [15]. Destructive methods are more precise but are not suitable for practical use, given their complex, time-consuming nature, and the fact that they destroy the battery. These methods are often used during development stages and research programs. In contrast, non-destructive techniques can offer detailed insights into a battery without damaging the battery.

One of non-destructive techniques is the charge and discharge method, which provides precise information about the battery health. However, it lacks information about the battery SOC as it fully charges and discharges the battery and consumes a significant time to perform.

As previously described, conventional EV BMSs passively monitor the cell voltages and currents and apply an algorithm to estimate parameters like SOC and SOH. While this approach is non-destructive, it lacks accuracy since its only based on passive measurements.

In contrast, electrochemical impedance spectroscopy (EIS) is an active, non-destructive method, that can provide a lot of information about the battery with more accuracy. This proven technique is fast and simple and commonly used by battery manufacturers for battery characterization. EIS measurements work by perturbing the battery with current and measuring the voltage response of the battery at different frequencies. The obtained complex impedance is than typically represented on a Nyquist plot. This method requires postprocessing of the measured data to extract the parameters of the battery from measurement. This work investigates the use of EIS for onboard battery characterization of an EV.

From an electrical point of view, a battery is a non-linear, time-dependent system. However, under stable operating conditions with a small signal perturbation, a battery can be approximated as a linear system with a well-defined impedance that does not change during measurement. In the model, the battery can be represented by the schematic diagram [8] shown in figure 2.3. In this model, $L1$ characterizes inductance of the battery, $R1$ characterizes the loss in the bulk electrolyte, $R2$ and $C2$ characterize the Ohmic loss and capacitance in the electrolyte-electrode interfaces, and Z_W is the Warburg impedance which represents diffusion loss at the electrode-electrolyte interface. Different characteristics of the battery, such as SOC, SOH, and temperature can be approximated from the values of the components in the circuit model. EIS provides a pathway to extract the circuit model from the measured impedance. The scope of this thesis focuses on measuring the battery impedance using EIS, and not on the details of equivalent circuit extraction.

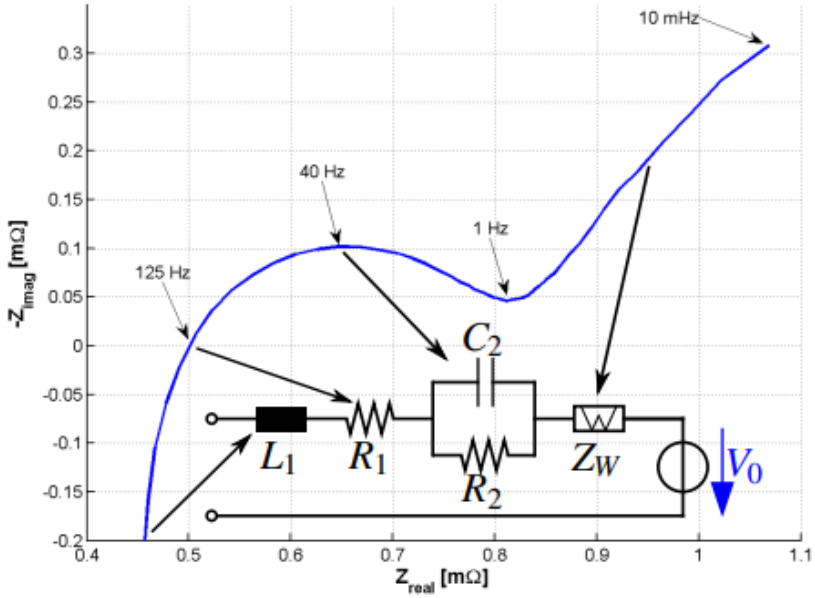

Figure 2.3: Schematic approximation of a battery with corresponding impedance at different frequencies - taken from[8]

2.4 Previous approaches to onboard EIS for EV battery monitoring

The technique to measure battery impedance is to perturb the battery with external current or voltage and measure the response. In a study from 2014 [3], a team of researchers used the motor controller as the excitation source. Although this is a cost-effective solution, the researchers ran into problems with accuracy and calibration. Also, this method requires intervention in the existing system and controller software. Another perturbation technique is to vary the duty cycle of a DC-DC power convertor connected to the battery as shown in [4]. However, a problem with this technique is that it can cause large voltage ripples at the output of power converter. In a study from 2021 [5] this issue is circumvented by inserting a small, switched resistor circuit into the converter to perturb the current. While this method requires an external circuit (increased bill of materials), it provides more precise impedance measurement than using a DC/DC power converter and significantly lowered the ripple.

In this study, the primary focus is to develop an addition to the BMS that provides real-time data on the battery's impedance. This addition provides an active onboard battery EIS measurement method that is both simple, lightweight and cost-efficient. It is similar to the approach used in [3] in that it involves an external circuit, but the proposed circuit can produce arbitrary current waveforms (including sinusoids and pulses of arbitrary durations, rise/fall times, and amplitudes), whereas the method in [3] can only pro-

duce simple pulses with a fixed amplitude. Therefore, this approach offers a straightforward and flexible solution to enhance the EV´s BMS, while offering ease and simplicity of implementation.

Chapter 3

Proposed Approach

3.1 The main idea

The basic idea of this project is to measure a battery's cell impedance by perturbing the battery with a known current and measuring the resulting change of the cell voltage. The impedance at a given frequency f can then be simply calculated using the following equation.

$$Z_{bat}(f) = \frac{V_{bat}(f)}{I_{bat}(f)} \tag{3.1}$$

Where the Z_{bat} is the wanted impedance of the battery, V_{bat} is the measured voltage (phasor) of the battery and I_{bat} is the measured current (phasor) that is drawn from the battery.

In this project, the basic idea for generating the perturbing current through the battery is to drive the gate of a MOSFET to modulate the load impedance seen by the battery as shown on the figure 3.1. The source of the gate voltage signal is external, for example a microcontroller or standalone waveform generator.

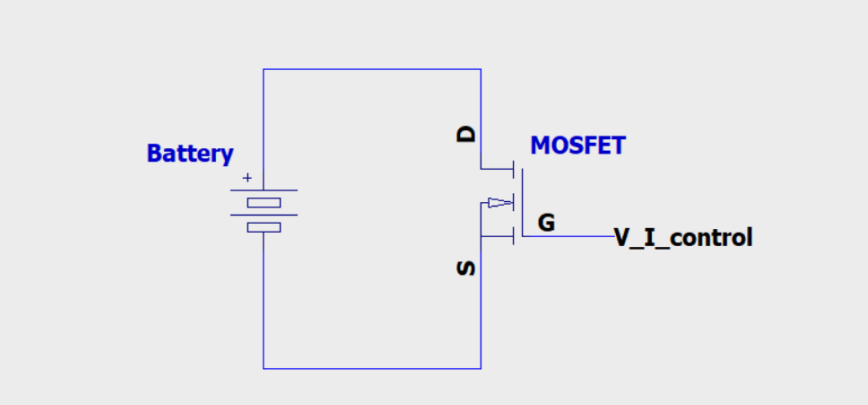

Figure 3.1: Basic idea for perturbing the battery current involves precisely discharging the battery cell driving the gate of a MOSFET.

3.2 Advantages of this approach

One of the most important features of this solution is that it is independent and modular, i.e., its operation does not rely on that of other existing systems or parts in the car. While implementing EIS using an existing part to perturb the current, such as the inverter or a DC/DC power converter, would reduce the overall part count, such an approach would come with significant disadvantages. As safety and compatibility of parts is crucial in the automotive industry, implementing any changes in the software of existing parts means that extensive testing of the new configuration is required, let alone changes in the hardware side of the parts. By creating an independent and modular system, we thus gain the opportunity to avoid these expensive and time-consuming tests that need to be performed. With that said, introducing a new part means that the part also has to be tested, however, due to its simplicity, the testing is not expected to be overly complicated or extensive. Modularity provides a host of other benefits as well, including easier maintenance and repair, scalability and upgradability, faster development and prototyping.

Another advantage of this solution being independent and modular is its independence on the state of other systems during operation. The EIS measurement can be done during driving, charging the battery, when the vehicle is parked and turned off or in nearly any other situation that the vehicle could need information about the battery modules to maximize range, performance or increase safety measures.

As another benefit, the solution does not use any switches and it works in linear mode. Therefore, it doesn't create any switching noise or higher harmonic signals that could cause problems with electro-magnetic compatibility within the vehicle. Also, it is expected to generate minimum noise that will not appreciably affect the precision of the measurement.

Moreover, using a simple circuit requires a small number of electrical components creating a lightweight part that does not significantly affect the overall weight of the already heavy EVs. In addition to that, the small number of electric components makes for a low-cost implementation.

3.3 Limitations of this approach

One limitation of this solution is that the battery is only being discharged. To perform the measurement, discharge waveforms with DC bias are created. In doing so, the current is discharged from the battery. However, the measurement is performed in a short amount of time. Even though the discharged current is relatively high, the short time period will ensure that the extracted

power will not be as significant.

As study from 2006 [6] shows, the difference between using charge or discharge direction of the current that perturb the battery has minimal effect on EIS and both charge and discharge methods are feasible for this application. Also study from 2018 [1] examine the influence of timescale on which is the measurement of the internal resistance of and lithium-ion cells performed. The research concludes that the interval from the start of the perturbation to the point on which is the measurement performed should be 4ms, but more commonly is use of 0.1s interval. In that study researchers used a fixed DC step. However, in this case the sinusoid signal is used to perturb the battery. Regarding that, the planned frequency range is under 2kHz, which aligns closely with the suggested range.

A method in study from 2004 [7] suggested that the frequency of perturbing signal of a battery should be in the mHz range. With that the precision will increase and the obtained data will be more relevant. Nonetheless using low frequency has downsizes as the signal may not be as stable and the spectrum could be less representative than using a more stable higher frequency range. Moreover, using low frequencies requires longer time to measure and the data are less representative as the actions in real use of the battery are not on the lower frequencies.

The study from 2014 [8] discusses and demonstrates the use of a DC/DC converter to generate signals that perturb the battery. The researchers implemented a filter to reduce noise from switching and inductance. As in the study mentioned before [4], they encountered problems with accuracy of the measurement. With that, the solution of this study that doesn't use any converter may benefit from the fact that there are no switches and relies on simple circuitry.

Chapter 4

Implementation

4.1 Circuit description

The complete EIS circuit schematic diagram is presented in figure 4.1. Note that the specific parts and reasons for choosing these parts will be discussed in the next section. In the circuit shown in figure 4.1, the first op-amp U1 is used as a part of the circuitry that adds a DC offset (red dashed box) to the input signal. This part of the circuit is optional. If the device performing the measurement is capable of adding a DC offset to the input signal, such that the signal values remain positive, then this part of the circuit can be removed.

The input signal is assumed to be a sine wave connected to pin V_{sin} and the DC offset voltage is applied to pin V_{DC} which should be equal to (or slightly greater than) the amplitude of the sinusoid input on V_{sin}. The peak-to-peak voltage of the sinusoid is assumed to be 400 mV. By using this voltage and a drain resistor $RS = 0.5\Omega$, the peak of the current through the main circuit is estimated to be around $I_{pk} = 400mV/0.5\Omega = 800mA$ Given the battery's published impedance ($70m\Omega$), this is expected to produce a reasonable voltage variation $\Delta V = 800mA \cdot 70m\Omega = 56mV$ on channel 2 (V_{CH2}). This configuration ensures sufficient resolution for precise measurements, aligning with the capabilities of typical spectrum analyzers and MCUs. Resistors $R3$ and $R4$ are used to scale the Input signal to correct values.

Op-amp $U2$ is used as a follower of the voltage on the source of MOSFET $M1$ and its output is connected to the gate of the $M1$. In combination with MOSFET $M1$, it controls the voltage across the reference resistor (RS) to be equal to the Input signal voltage. Resistor $R6$ is used to dissipate power which reduces the power dissipation of $M1$ as this MOSFET can overheat, especially during a long measurement with high current. To reduce the chance of overheating, small heatsinks are used on $M1$ and $R6$.

Resistors $R1$ and $R2$ function as a voltage divider for channel 2, enabling the measurement to be performed by a typical MCU. In this configuration, the maximum voltage on channel 2 is scaled down to compatibility with a 3.3V

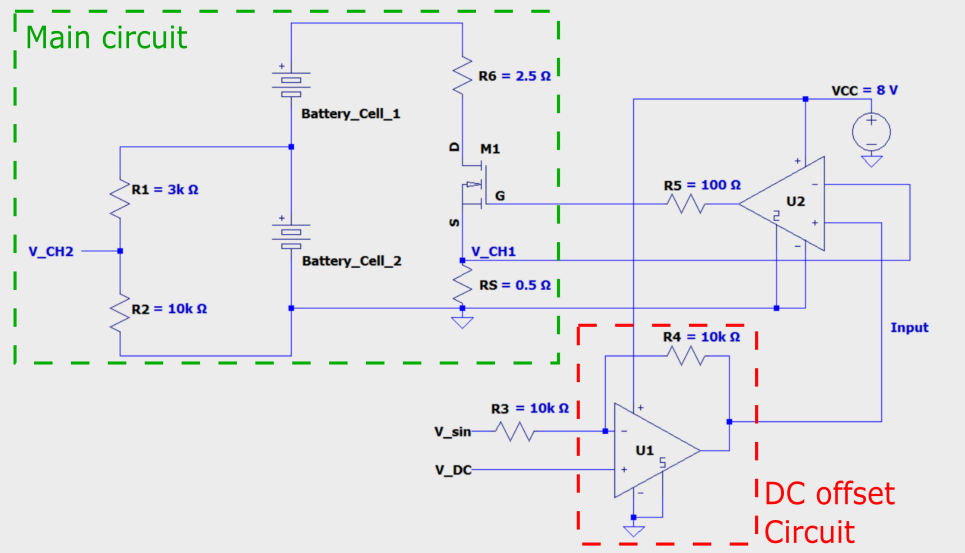

Figure 4.1: Full circuit diagram

architecture. To calculate the measured impedance of the battery cell 2, the following equation 4.1 is used.

$$Z_{bat}(f) = \frac{V_{CH2}}{V_{CH1}} \cdot R_S \cdot \frac{R_1 + R_2}{R_2} \tag{4.1}$$

Where Z_{bat} is the calculated impedance, V_{CH1} is the voltage measured on channel 1, V_{CH2} is the voltage measured on channel 2, R_S is the resistance of the reference resistor, and R_1 and R_2 are resistors used in voltage divider.

The op-amps can be powered either from an external source (Vcc) or directly from the batteries. For the sake of simplicity and to mitigate potential issues, an external source is chosen for this project. This decision is made to prevent complications that may arise from the battery pack, which consists of only two cells with a total voltage of $8V$ and a lower capacity. The output voltage of the batteries is susceptible to being affected by the current drained during the measurement process.

4.2 Part selection

4.2.1 Battery

Lithium-ion battery cells are chosen to measure in this work because lithium-ion batteries are the most commonly used battery type in electric vehicles [16]. However, instead of choosing a high-voltage EV battery pack, for safety and practical reasons two off-the-shelf commercial batteries connected in series

are chosen as device under test for EIS. Specifically, RS PRO ICR14500 [17] battery cells were selected for the following reasons:

1. Battery cell includes soldered wires on the terminals. Therefore, no external holders need to be used, eliminating contact resistance and other parasitic impedance that may occur between the battery and the holder.

2. The maximum output current of the battery cell is $2600mA$, which is sufficient for this application as the maximum peak excitation current for EIS measurement is below $1A$.

3. The battery initial impedance, measured at room temperature at 1 kHz, is rated at max 70mOhms. Combined with a perturbing current of $1A$ peak-to-peak, this creates a change in the voltage of the battery cell of $70mV$ peak-to-peak which is large enough to be sampled with a reasonable resolution using either a benchtop spectrum analyzer or ADC of a typical microcontroller.

4. According to the datasheet, the typical capacity of the battery cell is 820mAh, providing reasonable time to charge and discharge the battery which makes testing for different SOCs convenient. However, note that used EIS measurement approach is based on discharging the battery and may therefore influence the measurement if the battery cell's SOC changes appreciably during the measurement (especially at very low frequencies in the milli-Hz range). A battery with higher capacity would be potentially less viable to this inaccuracy.

4.2.2 MOSFET

For the MOSFET, which manages the current through the batteries, the IRLZ24NPBF [18] were chosen based on following parameters:

1. The threshold voltage is low enough to work within the given voltage range.

2. The drain-source resistance of $105m\Omega$ is low enough enabling the wanted current of $1A$ to flow through the resistor.

3. The maximum gate-source voltage is $16V$ and the maximum drain current is $18A$, which are both within the safe range for this application, considering the maximum voltage of the circuit is $8V$ and maximum current though the transistor is $1A$.

4.2.3 Op-amp

To regulate the voltage on the MOSFET gate, the LT1363 [19] operational amplifier was selected for the following reasons:

1. It supports single-rail power configuration, reducing the need for a negative power supply. Thanks to that, the op-amp can be powered by either a battery or an external DC power supply.

2. Both input and output types are rail-to-rail, allowing both input and output voltages to ground ($0V$) which is convenient and allows for a minimum DC offset of the discharge current.

3. The minimum supply voltage of $2.6V$ is suitable for this application, given that battery (series connection of two battery cells) is approximately $8V$. Furthermore, the maximum supply voltage of $44V$ provides the possibility of expanding to more battery cells.

4. The slew rate of $70mV/us$ is sufficient for this application.

5. The op-amp comes in the PDIP-8 package, which makes it suitable for both breadboard and soldering prototype boards.

4.2.4 Other components

The resistor models used in the circuit are selected according to their power rating, as some dissipate up to $5W$ and wide variety is used, ranging from $500m\Omega$ to $10k\Omega$. Bypass capacitors are used at the power pins of the op-amp to reduce inconsistency in power supply. Figure of circuit on the prototype board.

4.3 PCB design

A printed circuit board (PCB) was designed using KiCad, an open-source electronic design automation tool that allows creating PCB designs. This software was chosen for its free access, user-friendly and simple interface. The PCB, representing the circuit in figure 4.1, is designed as a two-layer board to accommodate all needed components and connections. The design is simplistic and can be condensed into a smaller package, yet it enhances understanding of the circuit and allows for the use of components with heatsinks. It features numerous ground points to facilitate connections with multiple measuring devices for testing the board. Additionally, the circuit features a ground plane as it is usually used to reduce crosstalk, enhance EMC performance, and provide a low-impedance and reliable return path. The 2D layout and 3D model of the PCB design are illustrated in figure 4.2 and figure 4.3 respectively.

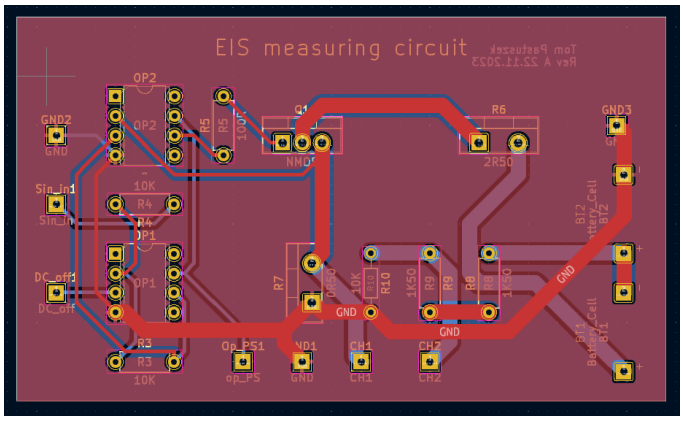

Figure 4.2: 2D KiCad model of the circuit

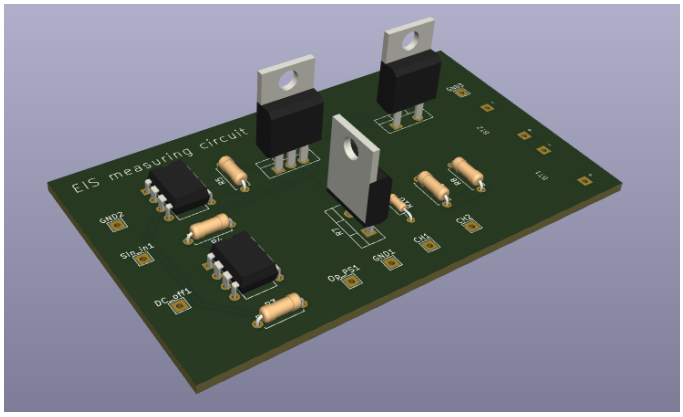

Figure 4.3: 3D KiCad model of the circuit

Note that the main focus in designing the PCB is to demonstrate what a production circuit would look like, providing insights into its size and cost estimation. As this work focuses on prototyping and validating the concept of onboard EIS measurement implementation, the PCB is not physically manufactured. Instead, only the version on the prototyping board, shown in figure 4.4, is made as it allows for convenient changes in the circuit, reducing cost and waiting time for new PCBs.

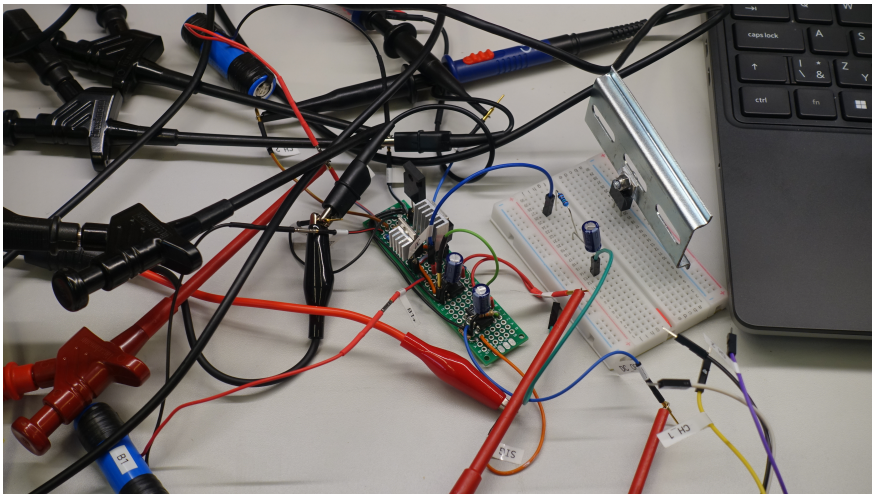

Figure 4.4: Measurements with prototype board

4.4 Bode100 spectrum analyzer

Testing is a crucial part during the development of a new idea. To ensure the circuit works as intended before implementing the measuring procedure on an MCU, a standalone laboratory device was used. This approach adds a certain precision, as errors are more likely to occur on the circuit itself than on the device used to perform the measurement. Moreover, the errors can be easily distinguished, making it easier to find their causes.

Figure 4.5: Omicron Lab Bode 100 spectrum analyzer - taken from [20]

As an external measuring device, Omicron Lab Bode100 [20] spectral analyzer was selected as it offers various measuring methods, including impedance analysis and frequency response analysis. Another reason for selecting this device was a simple fact, that this device is part of the equipment in the laboratory, where the circuit was tested. Moreover, Bode100 can generate sine waves of different frequencies and amplitudes, allowing it to be tuned as needed for the correct operation of the circuit.

One of the disadvantages of this device is that the frequency range starts at $1Hz$, which is not ideal as usually the measuring for EIS starts in mHz range. However, the measuring range for EIS extends up to kHz range, which is the device easily capable of. This provides a reasonable range to evaluate the functioning of the circuit.

Another disadvantage of Bode100 is that the mean value of the source sine waves is always $0V$. This is a major problem as the battery can't hold negative current through them and the circuit is not built to supply op-amps with negative voltage. To solve this problem, an easy solution was implemented in the form of adding DC offset to the source signal of the Bode100. This can be done by adding a second op-amp. The implementation of this additional circuitry can be seen on figure 4.1.

4.5 STM32 Nucleo

To create a real-time, on-board EIS measuring system and support the project objectives, the STM32 F303RE Nucleo [21] board is used to interface with the measuring circuit, replacing the Bode 100 laboratory device used for circuit evaluation. This specific microcontroller unit (MCU) is used due to its widespread use in the educational and development environment. Additionally, thanks to its affordability, any errors leading to board damage do not significantly impact the overall development cost.

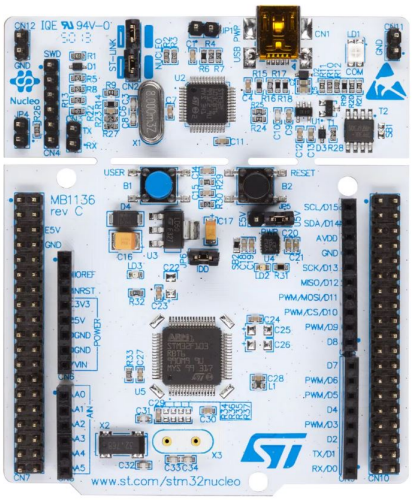

Figure 4.6: STM32 F303RE Nucleo board - taken from [22]

The programming language for the Nucleo is C. To create and compile the program running on the board, Studio Keil IDE was used with Mbed development platform. This compiler, provided directly by ST Microelectronics, supports all necessary libraries. The F303RE Nucleo features an ARM 32-bit

Cortex-M4 CPU, offering four 12-bit analog to digital converter (ADC) and two 12-bit digital to analog converters (DAC). In the implementation for this project, two ADC and one DAC are used.

The implemented program is designed to excite the EIS circuit with a sinusoidal signal generated from samples through DAC connected to pin PA_5 and measures the voltage levels of V_{CH1} connected to pin PA_0 and V_{CH2} connected to pin PA_1. All three pins are configured to analog output/input. The main loop sets the voltage on the output and uses the $wait()$ function to wait for one sample period. Afterward it samples the input signal of V_{CH1} and V_{CH2}. Note that the sample period is calibrated to include the time to change the output and to perform the reading of the voltages. The measured data is then exported through UART to a PC that is connected to the board using USB. The data is then exported to Excel table, from which it is used for post-processing.

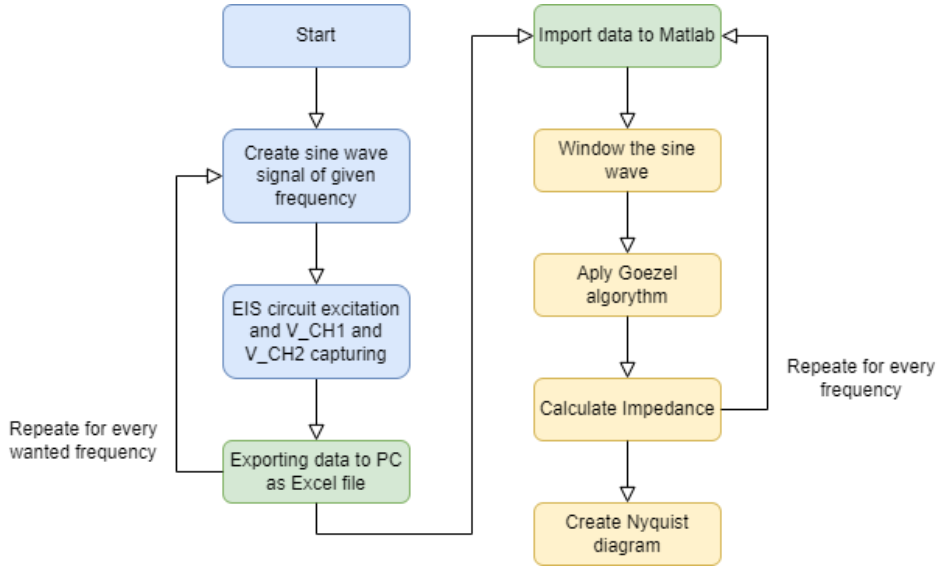

Figure 4.7: Flow chart of the measuring process using MCU

In the post-processing phase, magnitude and phase are calculated from the two sampled signals using MATLAB. This shift of post-processing from the MCU enables faster calculations, easier prototyping and allows for testing different methos of extracting the wanted parameters. The approach for this project entails extracting the phase from the sampled sine wave data by first windowing the signal, which smooths out abrupt changes of the sinusoid at the edges of the window, and then using the Goetzel algorithm. The results of this implementation are discussed in chapter 5 The C code for the F303RE Nucleo and MATLAB script are presented in Appendix A.

Chapter 5

Experiments and results

5.1 Circuit evaluation using Bode 100

To evaluate the accuracy of the voltage-controlled current sink circuit in conjunction with the Bode100 spectrum analyzer (employing the Bode 100 to generate the excitation sinusoid and measure the gain) for measuring impedance, a 500mOhm resistor was used as a device under test (DUT). The circuit was slightly modified to account for the DUT being a resistor rather than battery cells. To power the circuit, an external power supply was used. The modified circuit is shown in the figure 5.1.

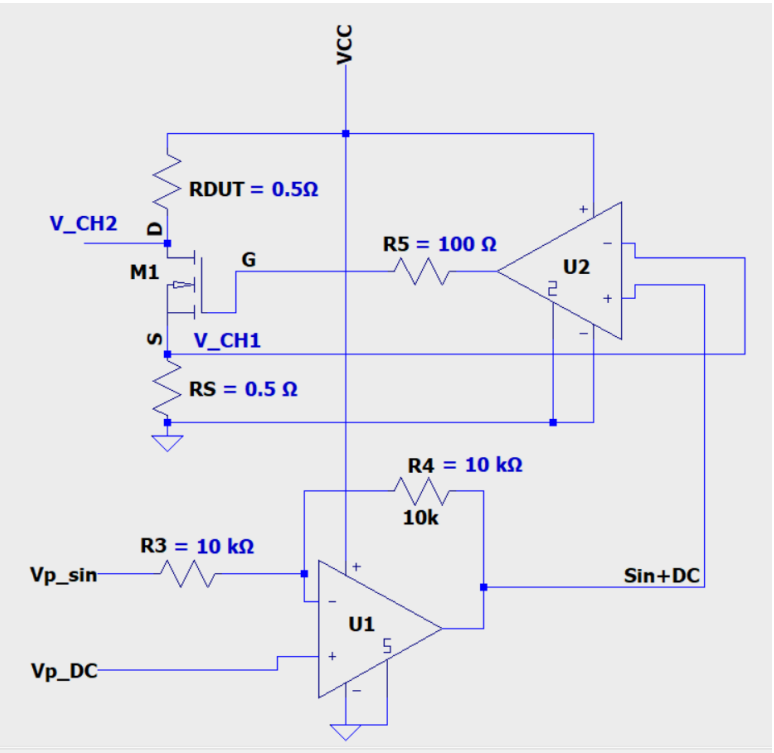

Figure 5.1: Diagram of modified circuit for resistor measurement

To measure the resistance of the DUT, the Bode100 was set to Gain/phase mode. This mode sweeps its output over frequency and measures the transfer function V_{CH2}/V_{CH1}. The Bode 100 was calibrated using the unit's through calibration procedure. Channel 1 and channel 2 are connected as shown in figure 5.1. The circuit was constructed on a breadboard as shown in figure 5.2. The resulting impedance is calculated by the equation 5.1.

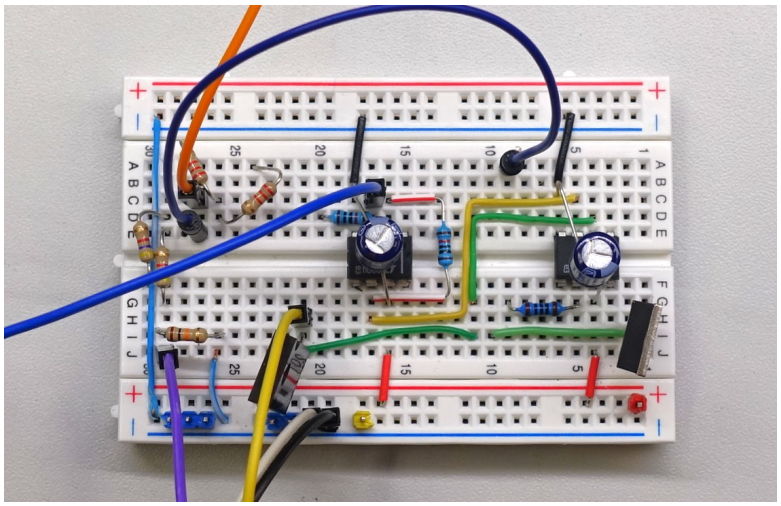

Figure 5.2: Breadboard prototype for resistor measurement

$$Z(f) = R_S \cdot \frac{V_{CH2}(f)}{V_{CH1}(f)} \tag{5.1}$$

Where $Z(f)$ is the resulting impedance, R_S is the resistance of the reference resistor and V_{CH1} and V_{CH2} are the measured voltages at the measuring points. The resistance is calculated by taking the real part of the impedance $Z(f)$.

Figure 5.3 shows a plot of the measured impedance magnitude. It is seen that around 1kHz the impedance rapidly increases. This resonance-like behavior is not due to the DUT, since the operating frequency is much less than the self-resonant frequency of this resistor. Instead, the resonant behavior is due to the "parasitic" impedance of the rest of the circuit connected to the DUT, including the parasitic inductance of the power supply cables, the power supplies input impedance, and the nonideal breadboard connections.

To remove this impedance, an additional calibration step was performed. The DUT resistor was replaced by a short circuit and a second measurement was performed to directly measure the "parasitic" impedance. This impedance

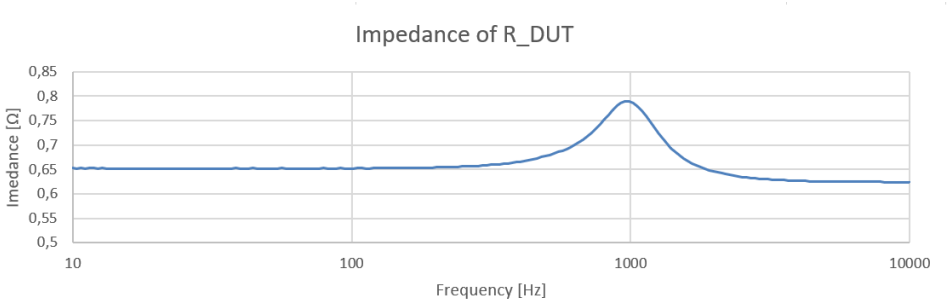

Figure 5.3: Measured impedance of resistor as DUT using breadboard prototype

was then subtracted out of the first measurement to obtain the impedance of the DUT resistor redirectly. The results of this measurement are shown in figure 5.4 (blue curve). For comparison, this figure also shows the resistance of the DUT measured directly using the Bode 100's impedance measurement mode with a B-WIC impedance adapter. The error between these two measurements is only 2.5%. Moreover, the measured resistance using the circuit presented is within the tolerance published in the resistor's datasheet [23], whereas the measurement obtained using the Bode 100's impedance measurement mode with the B-WIC impedance adaptor actually falls outside the manufacturer's published tolerance. Note that figure 5.4 shows the real part of the impedance (the resistance), and the imaginary part is not shown because of its negligible contribution to the overall impedance.

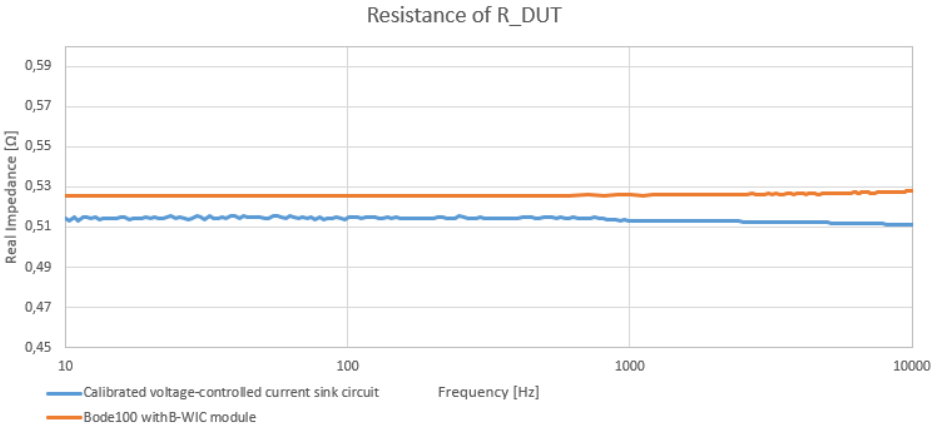

Figure 5.4: Measured resistance of DUT using B-WIC Bode 100 extension (orange) and using calibrated circuit (blue)

5.2 Battery measurement evaluation

To measure the impedance of a battery, the circuit shown in figure 4.1 is used in combination with the Bode 100 spectrum analyzer. As in the previous

section, the Bode 100 was set to Gain/phase mode and calibrated. The circuit was powered by an external power supply set to 8V. The Bode 100 was set to measure the Gain from 1Hz to 20kHz.

5.2.1 Battery impedance measurement at different SOC

The measurement at different states of charge (SOC) was done to validate the functionality of the circuit. To change the SOC, battery 2 was partially discharged between each measurement, starting from a full charge at 4.1V and concluding at approximately 20% SOC with a voltage of 3.43V. Following each discharge step, the battery was cooled to the laboratory temperature, given the highly sensitive nature of the battery impedance on temperature. The battery impedance values obtained for each open circuit voltage are graphically represented as a Nyquist plot in figure 5.5. Note that open circuit voltages are correlated to SOC – a lower (higher) the open circuit voltage indicates a lower (higher) SOC.

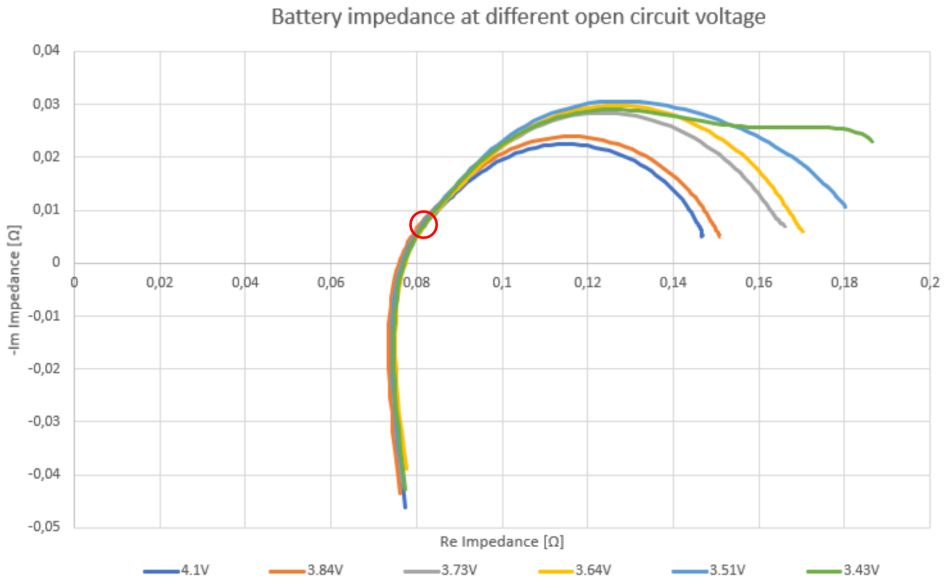

Figure 5.5: Nyquist diagram of measured battery impedance at different open circuit voltage

As evident from figure 5.5, the resistance increases (i.e., the Nyquist plot expands) as SOC decreases, as expected. A comparison with the results of a study from 2020 [24] on a Kokam lithium polymer pouch cell, shown in figure 5.6, reveals a similar trend to the measured results in this thesis. This agreement supports the presented EIS measurement technique and demonstrates its potential. Note that the Bode100 spectrum analyzer is not able to measure frequencies lower than 1Hz, whereas the results in [24], includes lower frequencies down to 10 mHz, which accounts for the characteristic rise in impedance at low frequencies shown in figure 5.6.

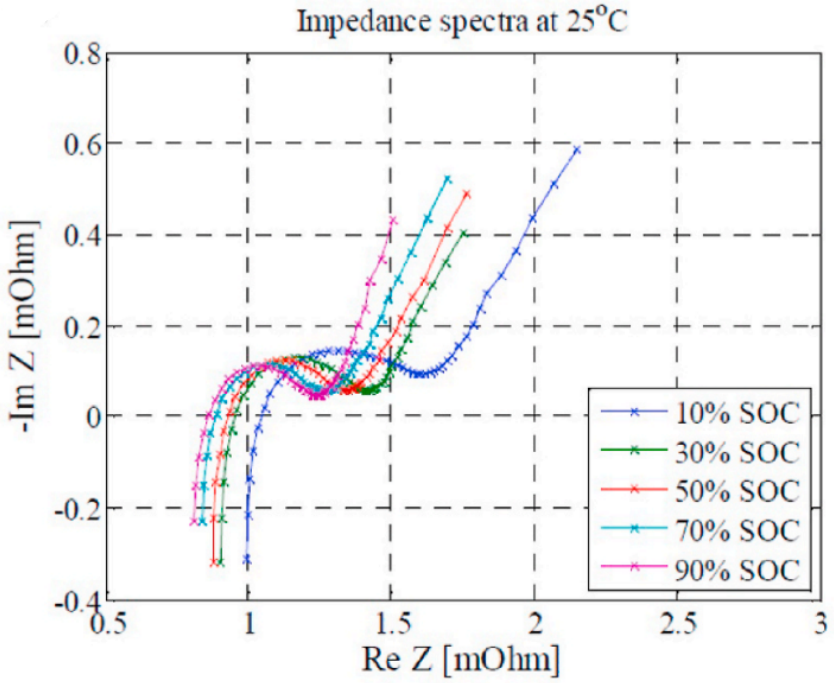

Figure 5.6: Nyquist diagram of measured battery impedance at different SOC from [24]

The impedance at 1 kHz is marked with a red circle for the 4.1V curve shown in figure 5.5. According to the battery specification [17], the maximum initial impedance is specified as 70mOhms. Initial impedance is typically defined at 1kHz. In this measurement, the impedance at 1 kHz remains relatively constant throughout the measured SOC range. The measured impedance is 82mOhms which is 17.1% off the value claimed by the manufacturer. There are a variety of potential causes for this deviation. The first cause of the error could be due to temperature. The manufacturer measures the initial impedance at a specific and controlled temperature (not specified in the battery's datasheet), whereas the measurement presented in figure 5.5 was performed at ambient laboratory temperature. Other causes of this deviation could be systematic measurement errors or the parasitic impedance of the wires and connections in the measuring circuit.

The best way to evaluate the measured data would be to compare them to reference data obtained from calibrated laboratory equipment. However, this equipment was unavailable during the time frame for this thesis, both within the company where the measurements were performed, and in the equipment available at the university.

5.2.2 Battery impedance measurement at different temperatures

The measurements at different temperatures were done to validate the functionality of the circuit. The DUT battery 2 was charged to an open circuit voltage of 4.1V and measured over a temperature range from 14 ^{o}C to 44.8 ^{o}C. To change the temperature, the battery was initially cooled in a refrigerator to achieve temperatures below the ambient temperature of the laboratory and then heated by heat gun to achieve temperatures higher than ambient temperature.

The battery cell´s temperature was measured using a thermal camera. This approach is not ideal, as the outside temperature of the battery can vary from the temperature inside the battery cell and the temperature is not uniform. To eliminate this problem as much as possible, the temperature was measured at the battery's electrode. The battery impedance values obtained for each temperature are graphically represented as a Nyquist plot in figure 5.7.

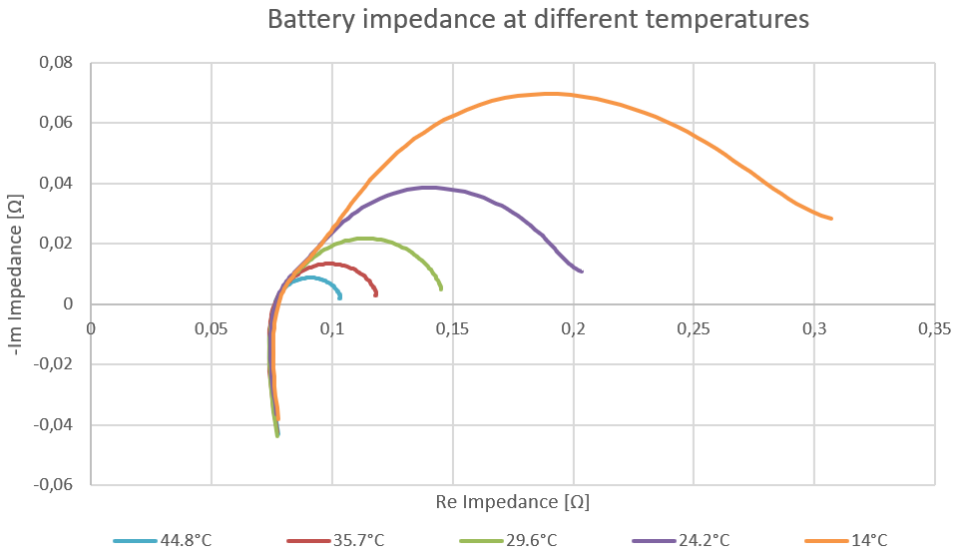

Figure 5.7: Nyquist diagram of measured battery impedance at different temperatures

As evident from figure 5.7, the resistance increases (i.e., the Nyquist plot expands) as the temperature decreases, as expected. A comparison with the results of a study from 2020 [24] on a Kokam lithium polymer pouch cell, illustrated in figure 5.8, reveals a similar trend to the measured results in this thesis. This agreement further supports the presented EIS measurement technique and demonstrates its potential. As shown in figure 5.7, the battery impedance is strongly dependent on the temperature, which underscores the importance of an TMS on battery performance. It is important to note that the battery temperatures shown in figure 5.7 are only indicative as the

temperature was not managed precisely, for example, by using a thermal bath. Moreover, the temperatures may have changed during the measurement.

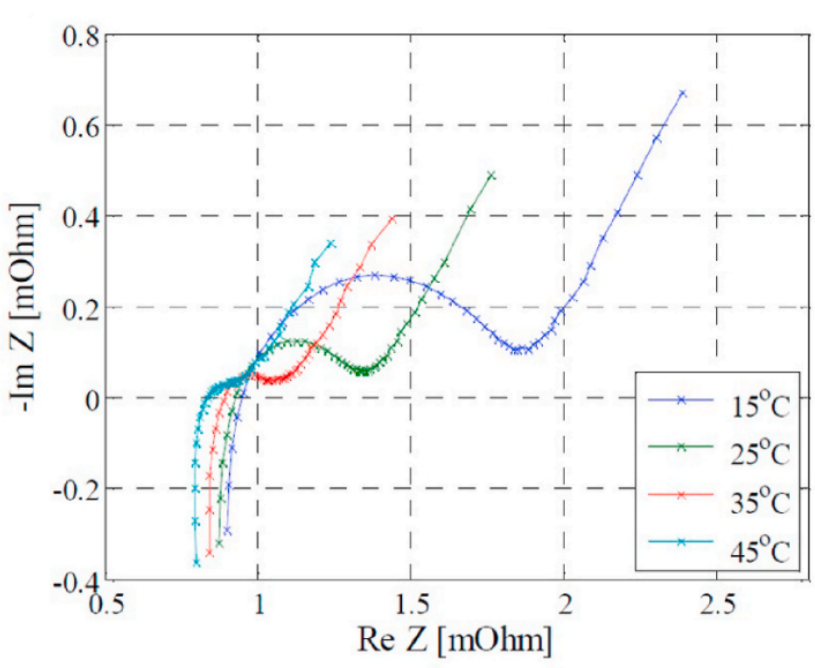

Figure 5.8: Nyquist diagram of measured battery impedance at different temperatures from [24]

5.3 Battery impedance measurement using MCU

In a realistic onboard EIS system, a microcontroller would be used in conjunction with the EIS circuit for battery impedance measurements (instead of a benchtop spectrum analyzer like the Bode 100). In this work, the STM32 F303RE Nucleo microcontroller is used in the prototype onboard EIS measurement system. The measurement starts at 2kHz, as this was the upper frequency limit achievable with the implemented approach and goes down to 50mHz. Measured data were exported to a PC using UART and then saved in an Excel table. From that, the data were exported to MATLAB, where they were post-processed to calculate phase and Impedance. The resulting Nyquist plot is presented in figure 5.9.

As seen in figure 5.9, the impedance at lower frequencies (on the right) follows the same trend as in figures 5.6 and 5.8 from the study [24]. However, at 2000Hz (on the left), the impedance deviates from the expected trend. This could be caused by an error in the measurement or by the limited precision

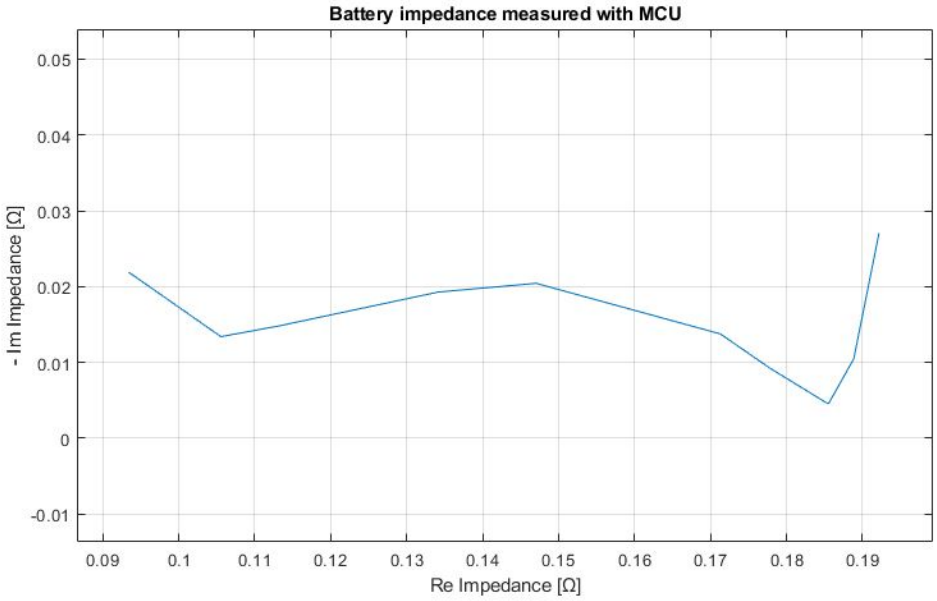

Figure 5.9: Nyquist diagram of measured battery impedance using MCU

of the MCU. Given its 12-bit ADC and operating range of 0 to 3.3V, one LSB is approximately 0.8mV, and the change in the measured voltage caused by the generated sinewave is only 40mV. In this scale, the measured data lacks precision. This quantization issue can be addressed by using a different MCU or external ADC with a higher resolution, or by increasing the voltage amplitude of the perturbing sine wave. However, such modification would also increase the power usage of the circuit, leading to an increase in heat that needs to be dissipated. This, in turn, increases cooling requirements and may result in the need for an active cooling system.

Further enhancement can be achieved by improving the precision of the sinewave generation, as the current implementation relies on the *wait*() function for sampling time. One technique which could provide more consistent sample times between samples involves replacing the wait function with an interrupt method. Alternatively, a PWM output and an RC filter can be used for sinewave generation, which eliminates the need for a DAC but adds high frequency switching noise. However, it is important to note that both methods may encounter limitations regarding the sampling speed of the ADC.

Despite the measured data using an MCU not matching the precision of results obtained with the Bode 100 spectrum analyzer, it still represents a noteworthy achievement. The results show the effectiveness of the implemented EIS-measurement technique for obtaining battery impedance data using the voltage-controlled current sink circuit and showcases the potential of such an implementation.

Chapter 6

Conclusion

6.1 Summary and results

In this thesis, a low voltage prototype of an EIS measurement system was developed to demonstrate its feasibility and identify opportunities and challenges for onboard battery EIS measurement for EVs. The prototype uses a voltage-controlled current sink to perturb the batteries. A sinusoidal signal is used as the input and the measured change in battery cell voltage is used to calculate the impedance of the battery. This measurement is performed for different frequencies to obtain the full Nyquist plot.

Two different versions of the prototype were built - one using Bode 100 spectrum analyzer and the other using STM32 F303RE Nucleo MCU. Using the Bode 100, a variety of measurements were performed at different battery SOCs and at different battery temperatures. The measurements show that the battery impedance is a function of SOC (i.e., impedance increases with lower SOC) and battery temperature (i.e., impedance decreases with higher temperatures). In particular, it was observed that battery impedance is highly sensitive to temperature change. Overall, the measurement results show a good agreement with what is expected based on similar measurements in the literature. Ideally, the measured results would be compared to reference measurements using a commercial battery impedance analyzer; however, such equipment was unavailable during this study. Using the MCU, the measured impedance at low frequencies matched expectations. However, at higher frequencies, the MCU´s 12-bit ADCs and perturbing implementation were slow and not precise enough to produce expected results.

Using the Bode 100, the measured initial impedance at 1kHz is approximately 17% higher than the expected value based on the battery´s datasheet. This difference may be attributed to factors such as a difference in battery temperature during measurement or other aspects of the measurement setup.

Overall, this work demonstrates the feasibility of using a voltage-controlled current sink circuit in an EIS measurement setup for acquiring battery impedance data. The circuit is relatively simple and cost effective, which showcases the

potential of this implementation for onboard EIS, thus establishing a solid foundation to build upon for future iterations.

6.2 Fulfilment of partial tasks of the thesis

The partial tasks of the thesis were fulfilled.

- Research battery management systems (BMSs) and EIS for EV batteries – elaborated in the chapter 2 and chapter 3
- Design an active current excitation circuit for online battery EIS. Apply this circuit with laboratory test equipment to measure the impedance spectra of lithium-ion battery cells – elaborated in sections 4.1 - 4.4 and evaluated in sections 5.1 and 5.2
- Develop a microcontroller-based EIS system prototype that manages the current excitation circuit, acquires current and voltage measurements, and generates the battery impedance spectra – elaborated in sections 4.5 and evaluated in section 5.3

6.3 Discussion and future work

Throughout the thesis, important insights have emerged. One of them is the emphasis on the precision of the circuit with which it is built, as it directly affects the precision of the measurement, and the environment in which the circuit is operated, as the battery impedance is highly sensitive to temperature changes. This stressed a need for better battery thermal regulation during the validation measurements, for example using a thermal bath.

A notable concern arises from the measuring duration, especially when operated in the milli-Hz range, lasting tens of seconds. For example, while measuring at a frequency of 50mHz and capturing 10 periods to create representative outcome, the duration of the measurement is equal to $T = 10 \cdot 1/(50 \cdot 10^{-3}) = 200s$. This extended duration poses potential challenges in real-time applications, as the battery can undergo significant discharging and charging during normal operation. Furthermore, within this time frame, the battery temperature may change, significantly influencing the precision of the measurement and potentially skewing the obtained results. In addition, the lower the frequency, the higher the discharge of the battery. For example, during the 10-period measurement at a frequency of 50mHz ($T = 200s$) with a maximum current peak of 800 mA, the battery is discharged 22mAh, which is about 2.7% from its full capacity (820mAh). While the percentage may seem significant, it is important to note that the battery cell used for testing has a significantly smaller capacity than those used in EVs.

One approach to provide stable and reliable results is to perform the measurement while the car is stationary or parked, eliminating the problem with

fluctuating battery charge during a measurement. However, this limits the usability of the technique, especially while obtaining the data to calculate remaining charge. Another option is to implement a complex algorithm that incorporates driving data concurrently with the impedance measurement process.

Another concern arises when scaling the prototype up to high voltages (800V), as a substantial power flow through the measuring circuit generates heat that requires dissipation. In this low voltage prototype (8V, 800 mA), the average dissipated power during an impedance measurement is calculated to be $1/2 \cdot 8 \cdot 0.8 = 3.2W$. This power is dissipated in the measurement circuit and requires heatsinks to dissipate the heat. For a high voltage (800V) system, the dissipated power would be around 320W. This requires a more sophisticated thermal management to keep the system at optimal temperatures. Especially when using a high voltage MOSFET.

Despite these challenges, this nondestructive and simple technique appears well-suited for onboard EV battery impedance monitoring. It offers crucial real-time information, such as SOC and temperature of battery cells, and holds the potential to enhance BMS compared to the current passive technique. Therefore, pursuing onboard EIS seems worthwhile, especially considering the advancements in machine learning and AI. These technologies could play a significant role in interpreting and utilizing the measured data for the BMS.

Bibliography

[1] Anup Barai, Kotub Uddin, W. D. Widanage, Andrew McGordon and Paul Jenning. A study of the infuence of measurement timescale on internal resistance characterisation methodologies for lithium-ion cells, January 2018. Available at: DOI:10.1038/s41598-017-18424-5

[2] Woosung Choi, Heon-Cheol Shin, Ji Man Kim, Jae-Young Choi and Won-Sub Yoon1. Modeling and Applications of Electrochemical Impedance Spectroscopy (EIS) for Lithium-ion Batteries. Journal of Electrochemical Science and Technology, January 2020. Available at: DOI: 10.33961/jecst.2019.00528

[3] David A. Howey, Member, IEEE, Paul D. Mitcheson, Senior Member, IEEE, Vladimir Yufit, Gregory J. Offer and Nigel P. Brandon. Online Measurement of Battery Impedance Using Motor Controller Excitation. IEEE Transactions on Vehicular Technology, vol. 63, no. 6, July 2014. Available at: DOI: 10.1109/TVT.2013.2293597

[4] Wangxin Huang, Student Member, IEEE, and Jaber A. Abu Qahouq, Senior Member, IEEE. An Online Battery Impedance Measurement Method Using DC–DC Power Converter Control. IEEE Transactions on Industrial Electronics, vol. 61, no. 11, November 2014. Available at: DOI: 10.1109/TIE.2014.2311389

[5] Qi Yao, Dylan-Dah-Chuan Lu and Gang Le. Accurate Online Battery Impedance Measurement Method with Low Output Voltage Ripples on Power Converters. Energies 2021, 14, 1064. Available at: DOI: 10.3390/en14041064

[6] Kazuo Onda, Masato Nakayama, Kenichi Fukuda, Kenji Wakahara and Takuto Araki. Cell Impedance Measurement by Laplace Transformation of Charge or Discharge Current–Voltage, April 2006. Available at: DOI: 10.1149/1.2189268

[7] A. Tenno, R. Tenno and T. Suntioc. A Method for Battery Impedance Analysis, April 2004. Available at: DOI: 10.1149/1.1697413

[8] Reinhold Koch, Robert Kuhn, Ilya Zilberman, Andreas Jossen. Electrochemical Impedance Spectroscopy for Online Battery Monitoring - Power Electronics Control, 16th European Conference on Power Electronics and Applications, Lappeenranta, Finland, August 2014. Available at: DOI: 10.1109/EPE.2014.6910907

[9] Statita. Market Insight, Electric vehicles - Worldwide. [online] Available at: `https://www.statista.com/outlook/mmo/electric-vehicles/worldwide` [cited on 2023-12-13]

[10] Virta. The state of EV charging infrastructure in Europe by 2030. Updated on 2023-10-5. [online] Available at: `https://www.virta.global/blog/ev-charging-infrastructure-development-statistics` [cited on 2023-12-13]

[11] Porsche Newsroom. The battery: Sophisticated thermal management, 800-volt system voltage. [online] Available at: `https://newsroom.porsche.com/en/products/taycan/battery-18557.html` [cited on 2023-12-13]

[12] Felix Govaers. Introductory Chapter: Kalman Filter - The Working Horse of Object Tracking Systems Nowadays, March 2019. Available at: DOI: 10.5772/intechopen.84804

[13] Angelo Maiorino, Claudio Cilenti, Fabio Petruzziello, Ciro Aprea. A review on thermal management of battery packs for electric vehicles, in Applied Thermal Engineering, vol. 238 February 2024. Available at: DOI: 10.1016/j.applthermaleng.2023.122035

[14] Min-Sheng Liu, Mark Ching-Cheng Lin, C.Y. Tsai, Chi-Chuan Wang. Enhancement of thermal conductivity with Cu for nanofluids using chemical reduction method, in International Journal of Heat and Mass Transfer, August 2006. Available at: DOI: 10.1016/j.ijheatmasstransfer.2006.02.012

[15] Uwe Tröltzsch, Olfa Kanoun, Hans-Rolf Tränkler. Characterizing aging effects of lithium ion batteries by impedance spectroscopy, in Electrochemica Acta, January 2006. Available at: DOI: 10.1016/j.electacta.2005.02.148

[16] C Iclodean1, B Varga, N Burnete, D Cimerdean, B Jurchiș. Comparison of Different Battery Types for Electric Vehicles, in IOP Conference Series: Materials Science and Engineering, 2017. Available at: DOI: 10.1088/1757-899X/252/1/012058

[17] Datasheet for RS Pro Rechargeable Lithium ion battery, RS Article:1834301 [online], Available at: `https://docs.rs-online.com/de49/0900766b816d2c0f.pdf` [cited on 2023-11-05]

[18] Datasheet for Infineon Technologies IRLZ24NPBF [online], Available at: `https://cz.mouser.com/datasheet/2/196/Infineon_IRLZ24N_DataSheet_v01_01_EN-3363548.pdf` [cited on 2023-10-13]

[19] Datasheet for Linear technology LT1363 [online], Available at: https://cz.mouser.com/datasheet/2/609/1363fa-3123210.pdf [cited on 2023-10-13]

[20] Datasheet for Omicron Lab Bode100 [online], Available at: https://www.omicron-lab.com/fileadmin/assets/Bode_100/Documents/Bode_100_R2_Technical_Data_V1.3.pdf [2023-12-17]

[21] Datasheet for STM32 F303RE Nucleo board [online], Available at: https://www.st.com/en/microcontrollers-microprocessors/stm32f303re.html [2023-12-29]

[22] Product page for STM32 F303RE Nucleo board [online], Available at: https://www.st.com/en/evaluation-tools/nucleo-f303re.html [2023-12-29]

[23] Datasheet for Bourns PWR221T-30 Series $500m\Omega$ power resistor [online], Available at: https://cz.mouser.com/datasheet/2/54/pwr221t_30-777826.pdf [cited on 2023-12-29]

[24] Nina Meddings, Marco Heinrich, Frédéric Overney, Jong-Sook Lee, Vanesa Ruiz, Emilio Napolitano, Steffen Seitz, Gareth Hinds, Rinaldo Raccichini, Miran Gaberšček, Juyeon Park. Application of electrochemical impedance spectroscopy to commercial Li-ion cells: A review. Journal of Power Sources, December 2020. Available at: DOI: 10.1016/j.jpowsour.2020.228742

Appendix A

Content of enclosed codes

Enclosed codes are presented in two folders

- *F303RE_ Nucleo_ code* This folder contains code for F303RE Nucleo board, that is responsible for perturbing and measuring voltages of the circuit.
- *Matlab_ postprocessing* This folder contains code to process data obtained by F303RE Nucleo board. It also contains raw measured data by this MCU.